Characteriazation and evaluation of synthetic Dawsonites as CO_2 sorbents

Fredrik Lundvall,[,†] Georgios N. Kalantzopoulos,[†] David S. Wragg,[†] Bjørnar Arstad,[§] Richard Blom,[§] Anja O. Sjåstad[†] and Helmer Fjellvåg[†]*

AUTHOR ADDRESS

† SMN - Centre for Materials Science and Nanotechnology, Department of Chemistry, University of Oslo, P.O. Box 1126, N-0318 Oslo, Norway

§ SINTEF Industry, P.O. Box 124, N-0314 Oslo, Norway

KEYWORDS

SEWGS, *in situ* X-ray diffraction, pre-combustion, CO_2 sorption, Rietveld, TGA, DSC, NMR

ABSTRACT

The sorbent enhanced water-gas shift (SEWGS) process has great potential for CO_2 capture and is thereby a realistic alternative to conventional post-combustion capture by gas emission scrubbing. Nevertheless, better performing materials are required to make SEWGS competitive against state-of-the-art scrubbing technologies. Dawsonite, $NaAl(OH)_2CO_3$, has a high carbonate content and forms *in situ* during CO_2 capture on alkali metal promoted alumina, thereby showing potential in variable temperature capture processes. For the isothermal SEWGS process the performance in pressure swing absorption is essential. We

evaluate here synthetic Dawsonites [MAl(OH)$_2$CO$_3$, M = K, Na] as CO_2 sorbents for the SEWGS process based on data from *in situ* X-ray diffraction, combined thermogravimetric analysis and mass spectrometry, magic-angle spinning nuclear magnetic resonance spectroscopy, as well as high pressure fixed bed reactor tests at isothermal conditions. The results show that synthetic Dawsonites are promising sorbents for the SEWGS process, however, with moderate cyclic CO_2 capacities (~0.3 – 0.7 mmol CO_2 / g sorbent) in comparison to alkali-metal promoted hydrotalcites. On the other hand, the materials exhibit relatively fast sorption rates at low temperatures (280 – 310 °C), favoring the water-gas shift reaction in the SEWGS process.

1. INTRODUCTION

Man-made emissions from power production contribute a significant portion of the annual worldwide emissions and increasing global CO_2 levels.[1] As energy production is likely to still rely on fossil sources for the near future, efficient technologies to clean flue gases of power plants are called for.[2] The sorbent enhanced water-gas shift (SEWGS) process is a pre-combustion CO_2 capture technology.[3-7] In such technologies, the fuel is decarbonized prior to utilization. One advantage is the potential of reaching 100 % CO_2 capture, compared to technologies like amine flue gas scrubbing which target capture values of ~90 %.[8] Pre-combustion capture is done by reforming the fuel to give a high pressure, syngas-rich (H_2 + CO) gas mixture. This gas mixture is then shifted towards higher H_2 yields through the water-gas shift (WGS) reaction ($CO + H_2O \rightleftharpoons CO_2 + H_2$). The WGS reaction is slightly exothermic ($\Delta H^0_{298K} = -41.1\, kJ/mole$) and hence thermodynamically limited under standard conditions.[9] Conventional WGS requires multiple cooling steps,[7] first from operating temperatures of about 400 to 200 °C for a second low temperature WGS reaction. The gas is cooled further to facilitate CO_2 absorption. By introducing an appropriate sorbent to the

process, CO_2 is captured *in situ* at operating temperatures, which shifts the equilibrium of the WGS reaction towards the desired product H_2. During sorbent regeneration through a pressure swing setup, the carbon from the fuel source is recovered as CO_2, providing decarbonized fuel for e.g. gas turbines (Figure 1).

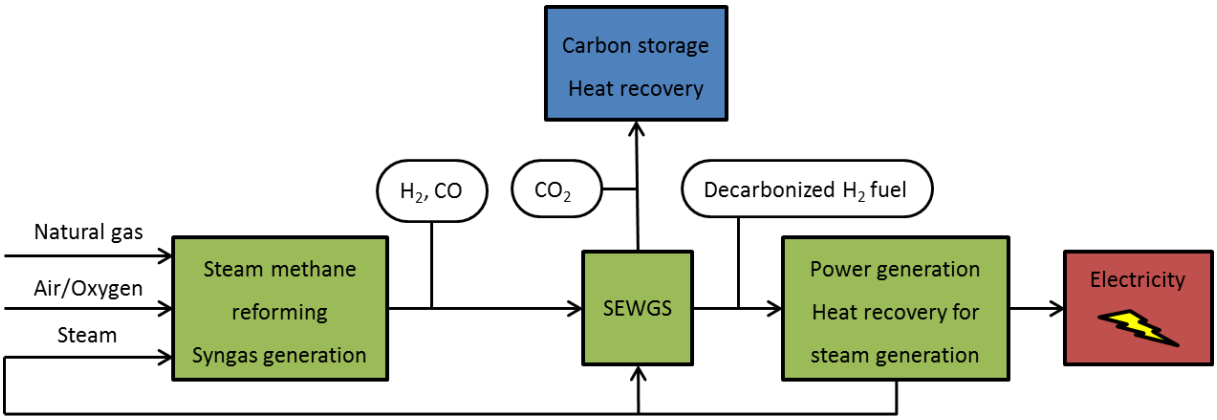

Figure 1: Schematic flow diagram of the sorbent enhanced water-gas shift (SEWGS) process.

Since the WGS reaction is exothermic, the equilibrium is shifted towards the product side at lower temperatures. On the other hand, the kinetics of the reaction strongly favor higher operating temperatures. Thus, an ideal sorbent for the SEWGS process should improve the kinetics of the WGS reaction while lowering the operating temperatures.

The mineral Dawsonite, $NaAl(OH)_2CO_3$, is of interest due to a relatively high gravimetric amount of carbonate in the structure. Dawsonite was discovered in 1862, described in 1875,[10-12] and structurally characterized in 1967.[13] The crystal structure comprises chains of edge-sharing octahedra of $AlO_2(OH)_4$ and $NaO_4(OH)_2$ oriented perpendicular to each other. Carbonate groups are located between chains, providing strength to the 3D structure through hydrogen bonding.[13, 14]

Dawsonite and related compounds can be produced synthetically, e.g. $MAl(OH)_2CO_3$, M = Na, K, NH_4. Other compositions have been reported, however Na-, K- and NH_4-Dawsonites dominate in the literature.[15] Naturally occurring crystals of Dawsonite display an acicular, or needle-like, morphology.[14] Synthetic K- and Na-Dawsonite display the same morphology,[16]

albeit with smaller crystallites (~30 × 250 nm and ~20 × 100 nm, Figure 2) that combine into large aggregated particles.

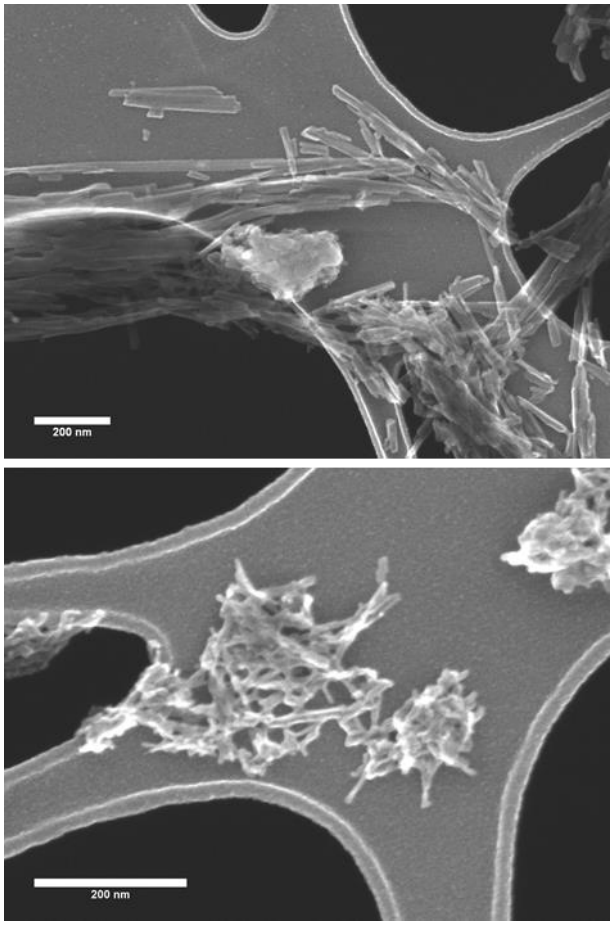

Figure 2: STEM images of a synthetic K- (top) and Na-Dawsonite (bottom).

The crystal structures of K- and NH_4-Dawsonite have clear similarities to that of the naturally occurring Na-Dawsonite (Figure 3). A common feature is the $AlO_2(OH)_4$ chains, however, there are significant differences in the arrangement of the monovalent cations. This leads to different space group symmetries (*Imma*, *Cmcm* and *Pnma* for Na-, K- and NH_4-Dawsonite, respectively).[17] For simplicity, we denote these compounds as Dawsonites despite the obvious structural differences.

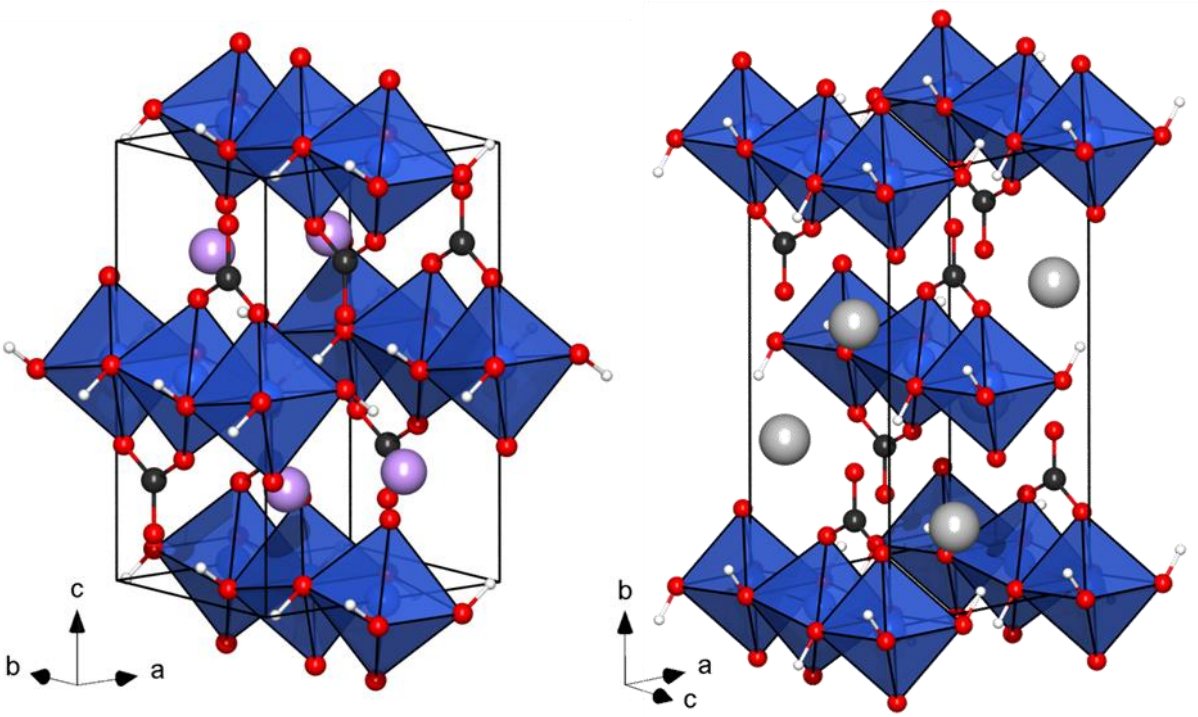

Figure 3: Comparison of Na-Dawsonite (left) and K-Dawsonite (right) (Al: blue, Na: purple, K: light grey, C: dark grey, O: red, H: white). Note the different crystallographic axes.

A recent publication reported on the *in situ* formation of Dawsonite from alkali metal promoted alumina used in the SEWGS process.[18] A second report details the potential of Dawsonite as sorbent in a temperature swing absorption process.[19] Inspired by these findings, we investigate here synthetic Dawsonites as CO_2 sorbent and assessed them for use in the isothermal SEWGS process.

2. EXPERIMENTAL

2.1. Materials and methods

Combined Thermogravimetric Analysis, Differential Scanning Calorimetry and Mass Spectrometry (TGA/DSC-MS) was performed on a Netzsch STA 449F1 under a flow of N_2-gas. The samples were heated from 30 to 800 °C in alumina crucibles, with a ramp rate of 2 °C/min. Variable temperature (VT) TGA/DSC was performed in platinum crucibles with a gas controller fitted to the instrument that enabled switching between two experimental gases. The instrument was set up with gas flows of 20 and 40 mL/min for the protective (N_2) and experimental (N_2 or CO_2) gas, corresponding to atmospheres of either 100 % N_2 or ~67 % CO_2 in N_2 at ambient pressure. The measurements were baseline corrected using the Proteus software package.[20]

Additional sorption analysis was performed in a custom-made pressure swing adsorption (PSA) rig under SEWGS relevant conditions.[21] The samples were activated at 350 °C in He for 60 minutes, and subjected to three absorption/desorption cycles at 280 and 350 °C, each cycle lasting for 60 and 240 minutes respectively (see Table 1). The partial pressures of CO_2 and H_2O were both 5 bar balanced with N_2 to a total pressure of 21.6 bar during absorption, and 5 bars of H_2O balanced with He to 21.6 bar during desorption.

VT and isothermal powder X-ray diffraction data (PXRD) were recorded at the Swiss-Norwegian Beamlines (BM01) at the European Synchrotron (ESRF), using monochromatic radiation (λ = 0.69264 Å; LaB_6 used as calibrant). The beamline is equipped with a Huber goniometer and a Dectris Pilatus 2M photon counting pixel area detector.[22, 23] The 2D diffraction data was converted to 1D PXRD diffraction patterns using Bubble.[23] The samples were ground in a mortar, filled in 0.5 mm inner diameter quartz capillaries in a flow cell and kept under a steady flow (~2 – 3 mL/min) of either N_2 or CO_2 during the experiments (see Figure S1 in ESI). In-house PXRD data were collected on a Bruker D8 instrument with

monochromatic CuKα_1 radiation (λ = 1.5406 Å) using a LynxEye XE position sensitive detector operated in transmission geometry. The VT data were visualized using Origin,[24] while Rietveld refinements and Pawley fits were performed using the TOPAS software.[25]

Nitrogen sorption measurements were performed on a BelSorp Mini instrument at 77 K. The samples were pre-treated for 2 hours at either 80 / 150 °C or 80 / 300 °C in a He atmosphere to remove gas species from the porous material.

Solid state nuclear magnetic resonance (NMR) experiments were performed at 11.7 T (500 MHz proton resonance frequency) using a Bruker Avance III spectrometer. The experiments used a 3.2 mm magic-angle spinning (MAS) probe at room temperature. The MAS rate was 20 kHz. ^{1}H spectra were acquired using the EASY pulse program.[26] For ^{27}Al spectra, single transient experiments were applied. The magnetic field was adjusted by setting the high frequency ^{13}C peak of adamantane to 38.48 ppm. The chemical shifts are referenced to tetramethylsilane and $Al(NO_3)_3$ according to the substitution method.[27] The samples were pre-treated for 1 hour at 150 °C and for 1.5 hours at 300 °C at low pressure (2.5 mbar) in a special glass apparatus enabling capping of the MAS rotors without exposure to air. The 300 °C treatment used the same sample that had been treated at 150 °C, keeping it under an Ar atmosphere between treatments.

Scanning Transmission Electron Microscopy (STEM) data were measured on a Hitachi SU8230 ultra-high resolution cold-field emission instrument.

2.2 Synthesis

All starting materials and solvents were used as received from commercial suppliers (Sigma-Aldrich and VWR). The syntheses of the Dawsonite samples were based on a literature procedure.[28]

2.2.1. Synthesis of K- and Na-Dawsonite

K-Dawsonite: $Al[OCH(CH_3)_3]$ (11.22 g, 48.54 mmol) was suspended in 100 mL of a saturated aqueous solution of $KHCO_3$ (33.0 g / 100 mL, ~33.0 g, 331.6 mmol).

Na-Dawsonite: $Al[OCH(CH_3)_3]$ (3.89 g, 19.05 mmol) and $NaHCO_3$ (9.60 g, 114.28 mmol) was suspended in 100 mL of a saturated aqueous solution of $NaHCO_3$ (solubility 9.6 g / 100 mL, ~9.6 g, 114.3 mmol).

The suspensions were stirred vigorously for 15 minutes before being heated in Teflon-lined steel autoclaves (Parr Instrument Company, acid digestion vessel model 4748A) at 120 °C for 48 hours. After cooling to room temperature, the resulting precipitates were remixed before the samples were again heated at 120 °C, now for 24 hours. The products were washed with de-ionized water by repeated centrifugations and resuspensions. Finally, the products were oven dried at 50 °C for 24 hours. The products were identified by PXRD analysis (see Figures S2, S3, and Table S1 in the ESI).

3. RESULTS AND DISCUSSION

3.1. Evaluation of the thermal stability of K- and Na-Dawsonite using TGA/DSC-MS and MAS-NMR

Samples of K- and Na-Dawsonite were investigated by combined TGA/DSC-MS analysis (Figure 4, and Figures S4 – S6 in the ESI). Despite the obvious structural differences between the two materials (Figure 3), the TGA/DSC-MS findings are remarkably similar. The decomposition of Na-Dawsonite is already treated in the literature,[29, 30] and therefore only K-Dawsonite will be discussed in detail.

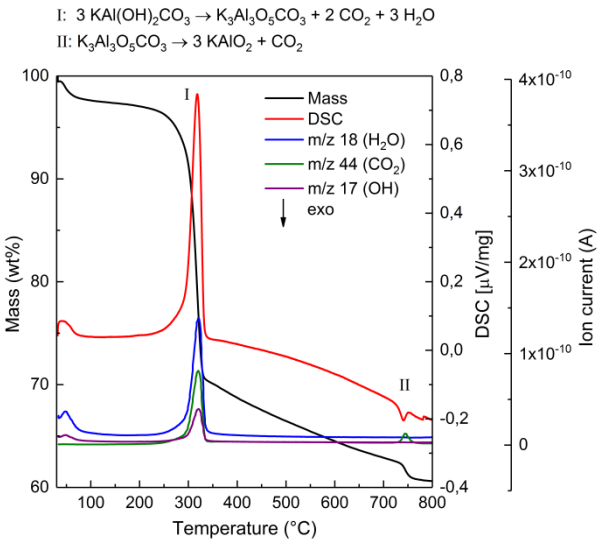

Figure 4: Combined TGA/DSC-MS analysis of K-Dawsonite. The two major chemical transformations are marked with roman numerals.

The TGA curve of K-Dawsonite shows several mass loss steps during heating. The first mass loss at 30 – 100 °C is attributed to surface bound water, based on the MS signal (m/z 18) and literature reports.[29-31] The next event is a substantial mass loss of about 27.1 wt% (29.6 wt% theoretical) occurring in the range 200 – 320 °C, with a particularly steep slope around 300 – 310 °C. The temperature range for this significant mass loss is consistent with literature findings,[29, 31-34] and concurrent with a sharp endothermic DSC signal and MS signals for m/z 17, 18 and 44 (OH, H_2O and CO_2). Less intense signals for masses m/z = 12, 16, 32 and 45

were also observed (C, O, O_2 and $^{13}CO_2$, see Figure S6 in ESI). From the MS signals we can see that the main contributors to the mass loss at 300 – 310 °C are hydroxyl, water and CO_2 (m/z 17, 18 and 44) originating from the carbonate and hydroxyl groups in the material.

In some reports, the main mass loss and endothermic events of synthetic K- and Na-Dawsonite are observed around 350 – 370 °C, which is significantly higher than our findings.[28, 35-40] Another report on natural Na-Dawsonite describes two separate endothermic events at 300 and 440 °C.[41] The reason for these discrepancies is not clear. However, the variations in thermal stability might be attributed to a difference between the hydrated and non-hydrated forms of the mineral,[37] or the larger particle size of the naturally occurring minerals.[40] Interestingly, the synthesis method also influences the material's stability. For instance, post-treatment in aqueous media,[32] or altering the reaction time during synthesis has an impact on the thermal stability.[39] The heating rate used in the thermal analysis does not appear to be a factor. It is therefore likely that the synthesis method used in the present work has a significant impact on the observed temperature for the main mass loss event.

Between 320 and 740 °C there is a slow mass loss of about 8.7 wt%. The DSC signal gives no clear indication for the type of the thermal event. The MS signals (Figure S6) are weak due to slow rate of evaporation, but do suggest release of species associated with carbonate. According to the literature, the Dawsonite sample should be fully dehydroxylated around 300 °C, as judged by infrared spectroscopy.[31] Note also that the sample exhibits poor crystallinity in this temperature range (see Figure S7 in the ESI).

Lastly, at 740 °C, there is a clear exothermic event and mass loss of about 1.6 wt% in the TGA/DSC signals. This is attributed to the transformation of the material into $KAlO_2$, the final decomposition product of K-Dawsonite (Figure S7). The transformation is associated with a clear signal for m/z = 44, caused by release of CO_2 from the remaining carbonate (Figure 4). The total mass loss for the three steps is 37.4 wt% which is in good accordance

with the theoretical value of 38.7 wt% for quantitative transformation of K-Dawsonite to $KAlO_2$. Note that the reported mass losses in wt% were normalized by setting the mass at 150 °C to 100 wt% to eliminate the mass contribution of surface bound water.

^{1}H and ^{27}Al MAS-NMR spectra were recorded as-synthesized samples, and after pre-treatment at 150 and 300 °C. At RT we expect to see contributions from both physisorbed water and hydroxyls coordinated to metal polyhedra. Curve fitting of the ^{1}H spectra in Figure 5 (see Figure S8 in ESI) reveals a compound peak at RT. It comprises a sharp peak at 4.5 ppm caused by physisorbed water and a broad underlying feature at 4.8 ppm assigned to hydroxyl groups. In addition there is a small peak at 2.9 ppm that is attributed to hydroxyl groups directly bonded to Al, and a peak at 3.7 ppm of unknown origin. After pre-treatment at 150 °C, the physisorbed water is removed, while significant dehydroxylation of the sample is unlikely. Curve fitting of the ^{1}H spectrum recorded after pre-treatment at 150 °C shows a broad peak at 4.6 ppm, a small peak at 2.4 ppm and a weak, yet distinct peak at 0.7 ppm. By superimposing the three spectra recorded at RT, 150 and 300 °C (see Figure S9 in the ESI), it is clear that the broad peak in the 150 °C sample strongly resembles the broad underlying peak at 4.8 ppm of the RT sample, supporting the assignment above. The moderate variations in chemical shift values between these two samples are due to subtle differences in hydrogen bonds depending on whether physisorbed water is present or not. The ^{27}Al spectra at RT and 150 °C are very similar (*vide infra*), further supporting no significant dehydroxylation at 150 °C.

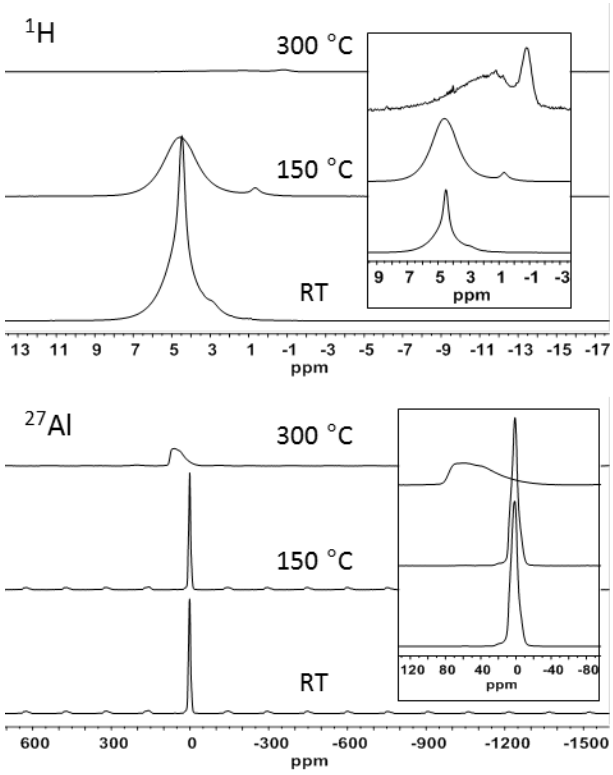

Figure 5: ^{1}H and ^{27}Al MAS-NMR spectra of K-Dawsonite. The panels show spectra of the samples as-synthesized, after heat treatment at 150 °C and at 300 °C (bottom, middle and top, respectively). The inserts show magnifications of the main peak. The peak heights are normalized in the ^{1}H spectra to highlight the 300 °C spectrum.

After heat treatment at 300 °C, the ^{1}H and ^{27}Al spectra change drastically. The total intensity of the ^{1}H spectrum is severely diminished compared to the spectra at RT and 150 °C. This is caused by dehydroxylation of the sample during this pre-treatment since the main peak in the 150 °C spectrum is attributed to hydroxyl groups. Despite the low total intensity there are features worth noting: a broad peak at around 1.8 ppm, and a sharp peak at −0.8 ppm. Conventionally, a broad hydroxyl peak is associated with a hydrogen bonded network, while a sharp hydroxyl peak indicates an isolated hydroxyl group.

In the ^{27}Al spectrum, the well-defined peaks at RT and 150 °C showing octahedrally coordinated Al atoms, have transformed into several broader and overlapping peaks with maxima around 68, 56, and 38 ppm. Using literature values, we have assigned the peaks at 68

and 56 ppm to four-coordinate Al and the peak at 36 ppm to five-coordinate Al.[42, 43] The pronounced tailing to the right is a strong indication of a distribution of quadrupolar couplings.

Complete MAS-NMR data for the Na-Dawsonite is reported in the ESI (Figures S10 – S12). These are qualitatively similar to the K-Dawsonite ^{1}H and the ^{27}Al spectra, with some notable differences. In the RT ^{1}H data, both samples display a sharp peak from physisorbed water at 4.5 ppm, whereas the peak attributed to hydroxyls is located at 5.8 ppm in Na-Dawsonite. The ^{27}Al NMR data from the RT and 150 °C samples indicates that the octahedrally coordinated Al in Na-Dawsonite experiences slightly higher electric field gradients compared to the K-Dawsonite since the peak shapes are less symmetric. Treatment at 150 °C removes in both cases the physisorbed water as described above. The samples treated at 300 °C have remarkably similar ^{1}H spectra considering the different shifts of most peaks except physisorbed water in the RT and 150 °C samples. In the Na-Dawsonite sample pre-treated at 300 °C, the ^{29}Al spectrum has a different shape, probably caused by a different relative distribution of four- and five-coordinate Al.

To the best of the authors' knowledge, the structure of the intermediate oxide carbonate present at 300 °C is unknown, and the ^{27}Al data suggests a rather complex structure. A "memory effect" and regeneration of the Dawsonite under certain conditions has been reported.[19, 44, 45] This, combined with the knowledge that the materials' surface areas are largely unaffected by loss of long range order, indicates that the intermediate likely has some similarity to the parent Dawsonite. Further analyses are necessary to map the subtle variations in the MAS-NMR spectra in detail to provide insight on the structure of the oxide carbonate intermediate.

Overall, the TGA/DSC-MS and MAS-NMR results are in agreement with the decomposition pathway suggested in the literature,[29, 30] where dehydroxylation and structural rearrangement occurs around 200 to 300 °C.

3.2. Sorption behavior of K- and Na-Dawsonite

With basis in the TGA/DSC-MS findings, the sorption properties of Dawsonite were explored in more detail. Recently, we reported on a TGA-based method for facile screening and evaluation of sorption properties of materials for SEWGS[46] by monitoring mass losses and gains during cycling of selected gases at specific temperatures. Absorption and desorption are correlated with exo- and endothermic events respectively, each in the range of about ±0.05-0.1 μV/mg, in the DSC signal of these studies (see Figure S13 in the ESI). This implies that chemisorption is likely the dominant sorption mechanism. The investigated materials show moderate surface areas of ~110 m^2/g and ~210 m^2/g (BET) for K- and Na-Dawsonite, respectively (see Table S2 in the ESI).

For the variable temperature sorption analysis, an initial activation step was applied by heating the sample to 350 °C at 5 °C/min, followed by cooling to 300 °C at 5 °C/min in a N_2-atmosphere. After holding at 300 °C for 60 min, the sample was cooled to the first temperature to be investigated, i.e. 250 °C, at a rate of 5 °C/min. After activation, the sample was subjected to three CO_2 absorption (60 min) and desorption (60 min) cycles. This cycling procedure was repeated at 10 °C intervals from 250 to 350 °C. In between each temperature isothermal, the sample was reactivated by heating to 350 °C at 5 °C/min. The result of the VT sorption experiments are shown in Figure 6 (top), where the TG curves have been normalized by setting the mass at 150 °C to 100 wt%.

The TGA data were analyzed to extract average absorption and desorption values. As example, individual absorption values were calculated by subtracting the lowest absolute value of the preceding desorption step from the maximum absolute value from the absorption step (equation 1).

$$(1)\quad wt\%_i^{abs} = wt\%_i^{max} - wt\%_{i-1}^{min}$$

The first absorption cycle after activation differs significantly from subsequent absorption cycles. Therefore, to ensure representative data, the minimum values of desorption cycles 1 and 2, and the maximum value of absorption cycles 2 and 3 were used for obtaining average sorption values. The results are plotted as a function of temperature to determine optimum conditions with respect to sorption capacity (Figure 6, bottom left).

Figure 6 (top) shows that the absorption and desorption curves differ notably in shape. In particular, the absorption curves approach saturation much faster than the desorption curves. To evaluate the kinetics at each isothermal, we applied a variant of the Tóth sorption equation to extract qualitative kinetic data (±A = theoretical $wt\%_{max/min}$, K = kinetic constant, t = time, c = heterogeneity coefficient, equation 2).[47, 48]

$$(2)\ wt\% = \pm A \frac{Kt}{(1 + (Kt)^c)^{1/c}}$$

The analysis was performed on the second sorption cycle of each isothermal. The values for K were extracted by setting the initial value for mass (wt%) to zero at recording time (t) zero (see Figure 6, bottom right, as well as Figure S14 and Table S3 in the ESI).

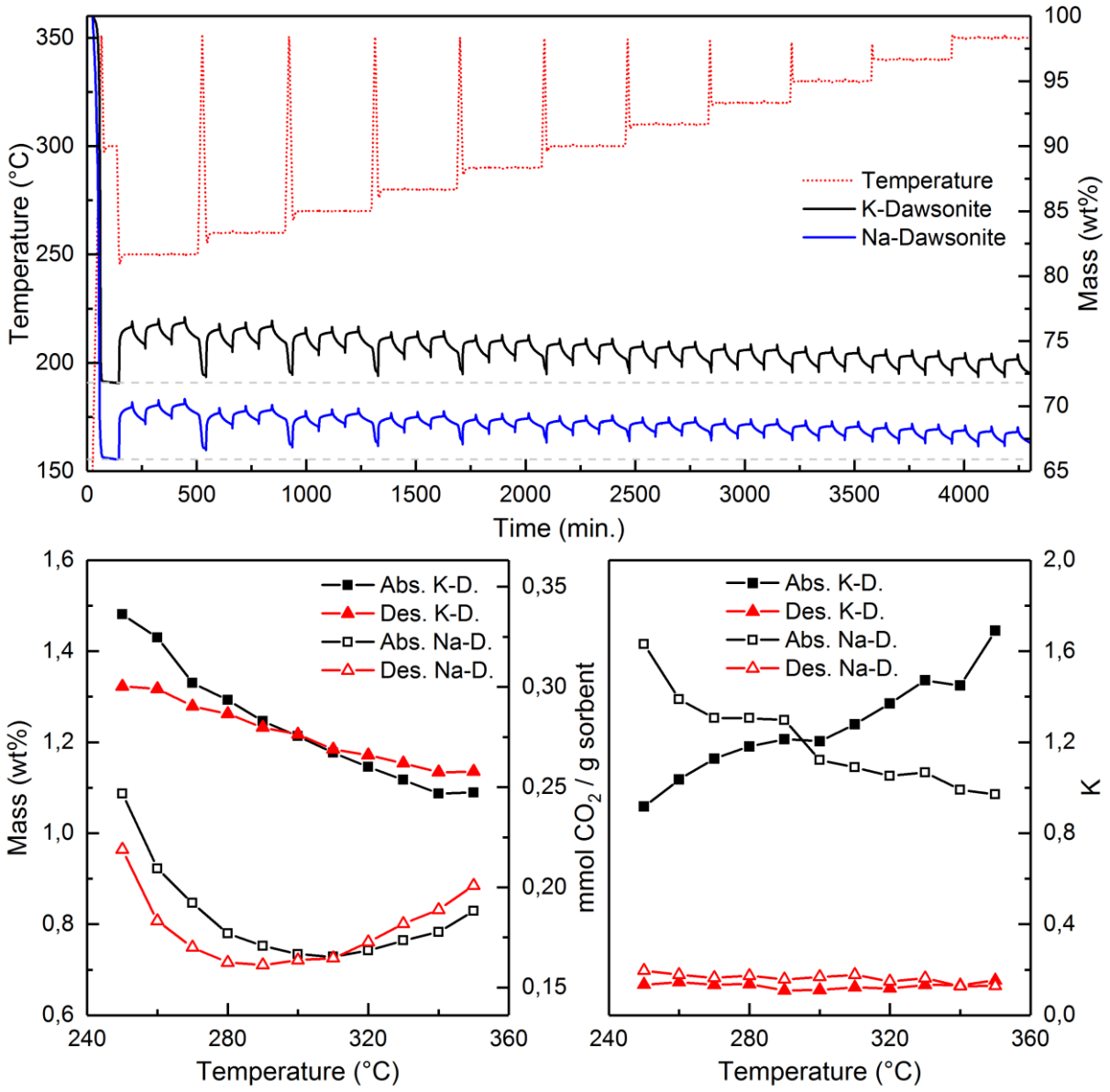

Figure 6: Graphs showing variable temperature CO_2 sorption analysis on K- and Na-Dawsonite. Top: Normalized TG curves of the two samples plotted against time, with grey dashed lines at 71.8 and 65.9 wt% indicating the lowest masses during the initial activation. Bottom left: Average sorption values of K- and Na-Dawsonite plotted against temperature. The error bars are omitted for readability since the error is smaller than 0.01 wt% in most data points and thus obscured by the data point symbol. Bottom right: K-values (indicating the kinetic speed of sorption) extracted from the Tóth analysis of the second sorption cycle at each isothermal, plotted against temperature.

The VT sorption analysis revealed both similarities and differences between Na- and K-Dawsonite. The top panel of Figure 6 shows that Na-Dawsonite reaches a lower initial mass after activation than K-Dawsonite. K-Dawsonite has a higher formula mass than Na-

Dawsonite (160.10 and 143.99 g/mol, respectively), and thus a slightly higher residual mass after activation (theoretically 70.4 and 67.1 wt%).

The materials show interesting differences in the cyclic sorption capacity (Figure 6, bottom left). K-Dawsonite has an overall higher cyclic sorption capacity (in mmol CO_2 / g sorbent) than Na-Dawsonite under these conditions. In addition, the cyclic sorption capacities of the Na- and K-materials have different temperature dependence. K-Dawsonite shows a diminishing sorption capacity with increasing temperature, whereas Na-Dawsonite shows a non-linear tendency, with an apparent minimum around 300 °C. It is unknown whether the sorption capacity of Na-Dawsonite will reach a plateau or start to diminish again at higher temperatures. We note that the absorption and desorption capacities of materials are similar at around 280 – 310 °C. This crossover point of the absorption and desorption curves is close to the temperature of the major mass loss event and structural rearrangements in both forms of Dawsonite.

High pressure sorption analysis at 280 and 350 °C under SEWGS relevant conditions[7, 21, 49, 50] (CO_2 / H_2O / N_2; 5 / 5 / 11.6 bar), reflect these findings (Table 1). At these conditions, both materials perform better at lower temperature, and there is a pronounced difference between the first and subsequent cycles. Interestingly, Na-Dawsonite appears to perform somewhat better with regards to absolute capacity at high pressure than at 1 bar.

Table 1: Results from high pressure sorption analysis. Data collected on a benchmark layered double hydroxide material is included for reference.

		CO_2 uptake (mmol CO_2 / g sorbent)		
Cycle	Temperature (°C)	K-Dawsonite	Na-Dawsonite	K-promoted LDH
1	280	1.07	1.03	1.49[a]
2	280	0.49	0.77	1.59[a]
3	280	0.54	0.69	1.61[a]
1	350	0.96	0.66	-
2	350	0.30	0.58	1.59
3	350	0.25	0.47	1.59

[a] average value of two measurements

Analysis of the cycling capacity curves with the Tóth equation (Figure 6, bottom right) reveals that the kinetic constant K is significantly (5 – 8×) higher for absorption than desorption in both samples. Consequently, absorption is a much faster process than desorption at all temperatures investigated. Furthermore, the kinetic constant for desorption is nearly equal for both materials and quite unaffected by temperature. This is reflected in the observation that both materials achieve 80 and 90% desorption in about 35 and 45 minutes respectively, regardless of temperature (see Figure S14 in the ESI). The kinetic constants for absorption show interesting variations; for K-Dawsonite they increase slightly with temperature, indicating faster initial absorption, while for Na-Dawsonite they decrease with increasing temperature. This indicates that the initial absorption rates of Na-Dawsonite slow down at higher temperatures. By comparison, 80 and 90% absorption is typically achieved in < 10 and < 20 minutes in the two samples. Moreover, the time needed to achieve 80 and 90% absorption decreases slightly with increasing temperatures in both samples (see Figure S15 in the ESI). These observations may explain the difference between K- and Na-Dawsonite with regard to cyclic sorption capacity as a function of temperature (*vide supra*).

Note that the A-parameters (theoretical $wt\%_{max/min}$) for desorption as derived from the Tóth equation implies that the materials should be able to desorb significantly more than observed and should in fact approach the value of the first absorption, assuming infinite holding time (Table S3). Consequently, the subsequent absorption value would then become higher. Sorption capacity as a function of time is a critical factor in evaluating materials for the SEWGS process. The current analysis shows that there will necessarily be a tradeoff between sorption time and capacity.

3.3. *In situ* analysis of the structural response of K-Dawsonite during sorption and heating

The thermal stability and sorption properties of K-Dawsonite were investigated *in situ* by synchrotron PXRD during heating and subsequent CO_2 sorption at a SEWGS relevant temperature (Figure 7). Each PXRD pattern is based on a 30 second exposure, ensuring decent temperature resolution while retaining good counting statistics. Based on the TGA data, the conditions for the sorption experiment had three main segments; activation, sorption, and thermal decomposition (Table 2).

Table 2: Conditions applied in the variable temperature PXRD experiment.

Segment	**Temperatures (°C)**	**Ramp rate (°C/min)**	**Gas**
I:N_2	RT → 300 → 280	5	N_2
II:CO_2	280	isothermal	CO_2
II:N_2	280	isothermal	N_2
III:CO_2	280 → 860	10	CO_2

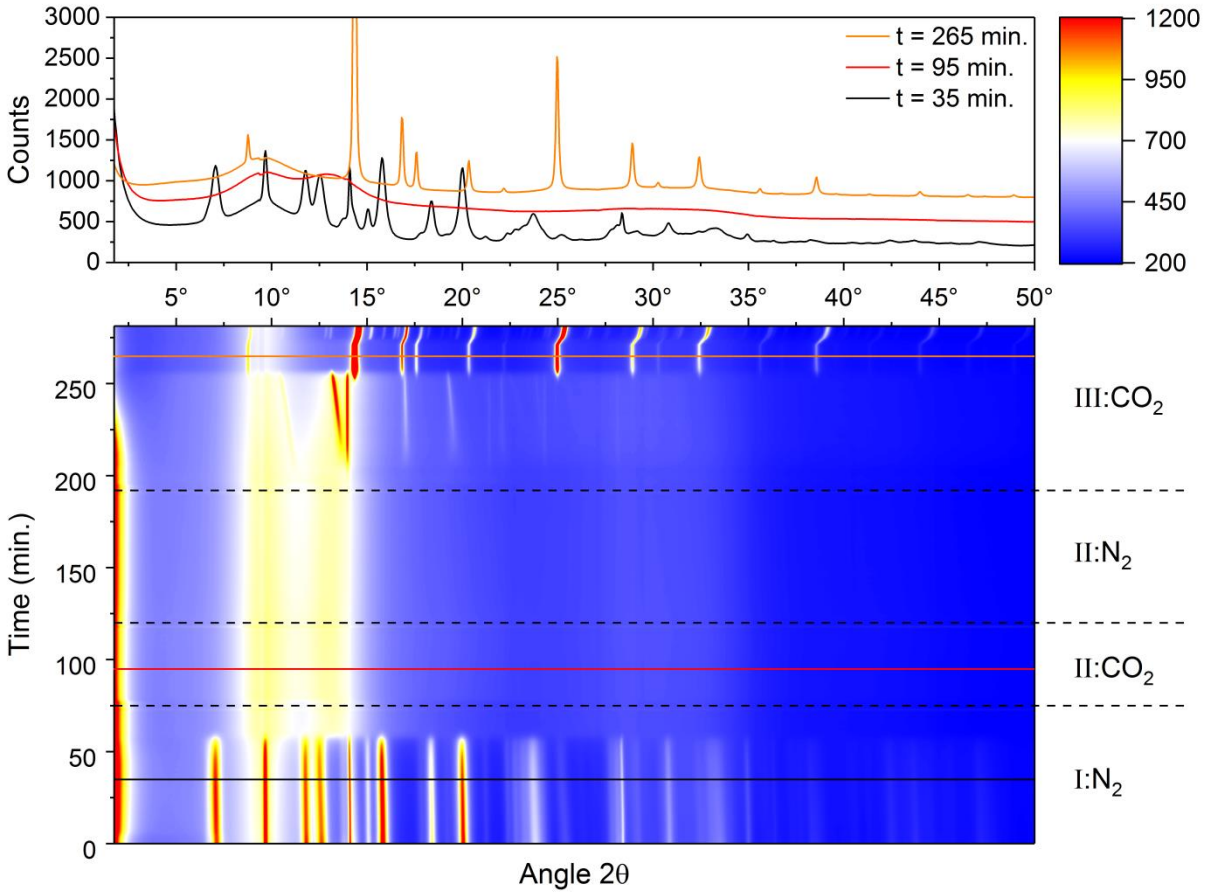

Figure 7: Contour plot of the VT PXRD measurement of K-Dawsonite (λ = 0.69264 Å). Selected patterns at 35, 95 and 265 minutes are indicated in black, red and orange respectively. The patterns are

staggered by a constant offset of 300 counts for clarity. Dashed black lines indicate a change of experimental gas.

In the first activation segment (Figure 7, I:N_2) the sample was heated to 300 °C at 5 °C/min, held for 5 minutes and then cooled to 280 °C. In this segment we see that as-synthesized K-Dawsonite remains crystalline up to around 300 °C (after ~60 min). A typical 1D diffraction pattern for K-Dawsonite is displayed in black in Figure 7. The loss of crystallinity coincides with the temperature where K-Dawsonite has the first significant loss of mass according to TGA data (Figure 4). Obviously, the long range order of Dawsonite is lost upon removal of hydroxyl and carbonate anions that are essential for 3D structure of the material.[13, 14]

The second segment of the VT experiment (Figure 7, II:CO_2 and II:N_2) describes the structural response during isothermal sorption of CO_2. A typical 1D diffraction pattern for this segment is displayed in red in Figure 7. The diffraction pattern corresponds to the active sorption phase which is poorly crystalline. This intermediate in the thermal decomposition of Dawsonite (*vide supra*) has earlier been described as "X-ray amorphous".[31] Although the material is lacking distinct long range order, it is not completely amorphous. Minor changes occur throughout the sorption experiment as determined by parametric profile refinements, which are indicative of short range order. The variation in peak positions of two broad main features show a clear evolution as function of time upon gas sorption (Figure 8).

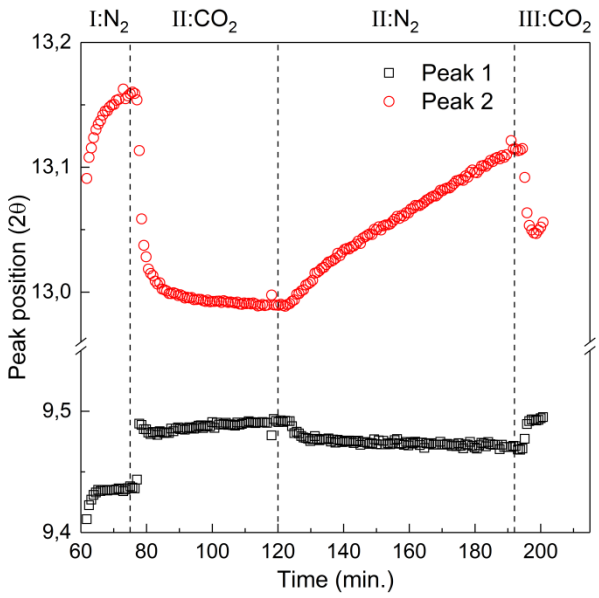

Figure 8: Peak positions of two main broad peaks in the diffraction pattern in segment 2 of the VT PXRD experiment. Dashed black lines indicate change of experimental gas.

The most distinctive response is observed in the peak at around 13.00 – 13.15°, which clearly shifts to lower angles during absorption. Correspondingly, the peak shifts to higher angles during desorption. This probably reflects slight changes in repeating layer separations when CO_2 is absorbed (swelling) or desorbed (shrinking). Similarly to the observations from the VT sorption experiments (Figure 6), there is an apparent difference in the kinetics of the absorption and desorption processes in the VT XRD experiments. The absorption process is relatively fast with maximum reached in less than 10 minutes, whereas desorption does not reach equilibrium within the 72 minutes of the experiment. A small delay in the response of 2-3 minutes is attributed to dead volume in the gas system. Furthermore, we observe a slight difference in the first and second CO_2 absorption cycles (t = 75 and 192). In the first absorption, the peak shifts some 0.15 degrees, whereas in the second absorption the shift is just 0.08 degrees. This is consistent with the significant differences between the first and subsequent absorption cycles observed in the VT sorption experiment (Figure 6). In addition

to these shifts, minor changes in the diffuse background scattering are observed throughout the experiment.

The third segment (Figure 7, III:CO_2) provides details on the structural response during heating in CO_2. The sample was held for 5 min at 280 °C before being heated to 860 °C at a rate of 10 °C/min, held for 5 min and finally rapidly cooled to room temperature. During heating, at around 450 °C, a set of sharp peaks emerge. The thermal expansion of this unknown intermediate phase, which is not present during heating in N_2 (see Figure S13 in the ESI), appears as unusually pronounced. At around 800 °C, the pattern changes dramatically as the material transforms into $KAlO_2$.[31, 40] The 1D diffraction pattern of $KAlO_2$ at 860 °C is displayed in orange in Figure 7.

4. CONCLUSIONS

In this article we have investigated and discussed the thermal stability and sorption properties of synthetic Dawsonites within the context of the SEWGS process. From our findings we conclude that Dawsonite has potential as sorbent for this emerging pre-combustion technology. We have demonstrated that the materials absorb and desorb CO_2 at SEWGS relevant temperatures. The sorption capacity is moderate (~0.3 – 0.7 mmol CO_2 / g sorbent), but the sorption rate is quite fast with 90% absorption typically achieved within 15-20 minutes. , giving a good cyclic sorption capacity as a function of time. More importantly, the highest sorption capacity is achieved at a relatively low temperature, 280 – 300 °C, which is favorable for the slightly exothermic water-gas shift reaction. A variable temperature PXRD experiment revealed that the active sorption phase under these conditions is a poorly ordered material that forms after the initial activation of the as-synthesized Dawsonites.

ACKNOWLEDGEMENTS

We acknowledge the support from the Research Council of Norway (project #190980), Interreg (MAX4FUN – UIO007) and the Department of Chemistry at UiO. The use of the Norwegian national infrastructure for X-ray diffraction and scattering (RECX) is highly acknowledged. We acknowledge the skilled staff at the Swiss-Norwegian beamlines at the ESRF. Ruth Elisabeth Stensrød, Dr. Silje Fosse Håkonsen and Joanna Pierchala, SINTEF, are acknowledged for recording TGA/DSC-MS data and performing high pressure sorption analysis. Kristian Blindheim Lausund is acknowledged for recording the STEM images.

REFERENCES

(1) Figueroa, J. D.; Fout, T.; Plasynski, S.; McIlvried, H.; Srivastava, R. D., *Int. J. Greenhouse Gas Control* **2008**, *2*, 9-20.
(2) Schrag, D. P., *Science* **2007**, *315*, 812-813.
(3) Hufton, J. R.; Mayorga, S.; Sircar, S., *AIChE J.* **1999**, *45*, 248-256.
(4) Hufton, J. R.; Allam, R. J.; Chiang, R.; Middleton, P.; Weist, E. L.; White, V., Development of a process for CO_2 capture from gas turbines using a sorption enhanced water gas shift reactor system in *Greenhouse Gas Control Technologies 7*, Rubin, E. S.; Keith, D. W.; Gilboy, C. F., Eds. Elsevier Science Ltd; Oxford **2005**, 253-261.
(5) Gazzani, M.; Macchi, E.; Manzolini, G., *Fuel* **2013**, *105*, 206-219.
(6) Manzolini, G.; Macchi, E.; Gazzani, M., *Fuel* **2013**, *105*, 220-227.
(7) Jansen, D.; van Selow, E.; Cobden, P. D.; Manzolini, G.; Macchi, E.; Gazzani, M.; Blom, R.; Henriksen, P. P.; Beavis, R.; Wright, A., *Energy Procedia* **2013**, *37*, 2265-2273.
(8) Rochelle, G. T., *Science* **2009**, *325*, 1652-1654.
(9) Ratnasamy, C.; Wagner, J. P., *Catal. Rev.: Sci. Eng.* **2009**, *51*, 325-440.
(10) Harrington, B. J., *Can. Natural. and Quart. J. Sci.* **1875**, *7*, 305-309.
(11) Harrington, B. J., *Can. Natural. and Quart. J. Sci.* **1883**, *10*, 84-86.
(12) Stevenson, J. S.; Stevenson, L. S., *Can. Mineral.* **1965**, *8*, 249-252.
(13) Frueh Jr, A. J.; Golightly, J. P., *Can. Mineral.* **1967**, *9*, 51-56.
(14) Corazza, E.; Sabelli, C.; Vannucci, S., *Neues Jahrbuch für Mineralogie, Monatshefte* **1977**, 381-397.
(15) Yalfani, M. S.; Santiago, M.; Perez-Ramirez, J., *J. Mater. Chem.* **2007**, *17*, 1222-1229.
(16) Zhang, X.; Wen, Z.; Gu, Z.; Xu, X.; Lin, Z., *J. Solid State Chem.* **2004**, *177*, 849-855.
(17) Łodziana, Z.; Stoica, G.; Pérez-Ramírez, J., *Inorg. Chem.* **2011**, *50*, 2590-2598.
(18) Walspurger, S.; Cobden, P. D.; Haije, W. G.; Westerwaal, R.; Elzinga, G. D.; Safonova, O. V., *Eur. J. Inorg. Chem.* **2010**, *2010*, 2461-2464.
(19) Martin, O.; Hammes, M.; Mitchell, S.; Perez-Ramirez, J., *Energy Environ. Sci.* **2014**, *7*, 3640-3650.
(20) *NETZSCH Proteus 5.2.1*, NETZSCH Gerätebau GmbH: **2011**.
(21) Bakken, E.; Cobden, P. D.; Henriksen, P. P.; Håkonsen, S. F.; Spjelkavik, A. I.; Stange, M.; Stensrød, R. E.; Vistad, Ø.; Blom, R., *Energy Procedia* **2011**, *4*, 1104-1109.
(22) Broennimann, C., *Acta Crystallogr., Sect. A: Found. Crystallogr.* **2008**, *64*, C162.
(23) Dyadkin, V.; Pattison, P.; Dmitriev, V.; Chernyshov, D., *J. Synchrotron Radiat.* **2016**, *23*, 825-829.
(24) *Origin 9.4.2*, Originlab Corp.: **2017**.
(25) *TOPAS 5.0*, Bruker AXS: **2014**.
(26) Jaeger, C.; Hemmann, F., *Solid State Nucl. Magn. Reson.* **2014**, *57*, 22-28.
(27) Harris, R. K.; Becker, E. D.; Cabral de Menezes, S. M.; Goodfellow, R.; Granger, P., *Solid State Nucl. Magn. Reson.* **2002**, *22*, 458-483.
(28) Li, X.; Ye, J.; Lin, Y.; Fan, L.; Pang, H.; Gong, W.; Ning, G., *Powder Technol.* **2011**, *206*, 358-361.
(29) Hernandez, M. J.; Ulibarri, M. A.; Cornejo, J.; Peña, M. J.; Serna, C. J., *Thermochim. Acta* **1985**, *94*, 257-266.
(30) Álvarez-Ayuso, E.; Nugteren, H. W., *Water Research* **2005**, *39*, 2096-2104.
(31) Huggins, C. W.; Green, T. E., *Amer. Mineral.* **1973**, *58*, 548-550.
(32) Stoica, G. *"Chemistry of Dawsonites and application in catalysis."* PhD thesis, Universitat Rovira I Virgili, Tarragona, **2010**.
(33) Stoica, G.; Pérez-Ramírez, J., *Geochim. Cosmochim. Acta* **2010**, *74*, 7048-7058.
(34) Loughnan, F. C.; See, G. T., *Amer. Mineral.* **1967**, *52*, 1216-1219.
(35) Kim, B. H.; Kato, C., *Nippon Kagaku Kaishi* **1974**, *1974*, 2075-2080.

(36) Kim, B. H.; Ishikawa, H., *Nippon Kagaku Kaishi* **1974**, 1417-1420.
(37) Fernández-Carrasco, L.; Rius, J., *Eur. J. Mineral.* **2006**, *18*, 99-104.
(38) Földvári, M., *Handbook of thermogravimetric system of minerals and its use in geological practice* Geological Institute of Hungary; Budapest, Hungary **2011**, Vol. 213.
(39) Zhang, X.; Wen, Z.; Gu, Z.; Xu, X.; Lin, Z., *Thermochim. Acta* **2005**, *433*, 116-120.
(40) Harris, L. A.; Ernst, W.; Tennery, V. J., *Amer. Mineral.* **1971**, *56*, 1110-1113.
(41) Beck, C. W., *Amer. Mineral.* **1950**, *35*, 985-1013.
(42) Fitzgerald, J. J.; Piedra, G.; Dec, S. F.; Seger, M.; Maciel, G. E., *J. Am. Chem. Soc.* **1997**, *119*, 7832-7842.
(43) Zhang, W.; Bao, X.; Guo, X.; Wang, X., *Catal. Lett.* **1999**, *60*, 89-94.
(44) Stoica, G.; Groen, J. C.; Abelló, S.; Manchanda, R.; Pérez-Ramírez, J., *Chem. Mater.* **2008**, *20*, 3973-3982.
(45) Stoica, G.; Pérez-Ramírez, J., *Chem. Mater.* **2007**, *19*, 4783-4790.
(46) Lundvall, F.; Kalantzopoulos, G. N.; Wragg, D. S.; Arstad, B.; Blom, R.; Olafsen Sjåstad, A.; Fjellvåg, H., *Energy Procedia* **2017**, *114*, 2294-2303.
(47) Tóth, J., *Adv. Colloid Interface Sci.* **1995**, *55*, 1-239.
(48) Kalantzopoulos, G. N.; Antoniou, M. K.; Enotiadis, A.; Dimos, K.; Maccallini, E.; Policicchio, A.; Colavita, E.; Agostino, R. G., *J. Mater. Chem. A* **2016**, *4*, 9275-9285.
(49) Wright, A. D.; White, V.; Hufton, J. R.; Quinn, R.; Cobden, P. D.; van Selow, E. R., *Energy Procedia* **2011**, *4*, 1147-1154.
(50) van Dijk, E.; Walspurger, S.; Cobden, P. D.; van den Brink, R. W., *Energy Procedia* **2011**, *4*, 1110-1117.